Optical Conductivity of the Holstein Polaron

Glen L. Goodvin,[1] Andrey S. Mishchenko,[2,3] and Mona Berciu[1]

[1]*Department of Physics & Astronomy, University of British Columbia, Vancouver, British Columbia, Canada, V6T 1Z1*
[2]*Cross-Correlated Materials Research Group (CMRG), ASI, RIKEN, Wako 351-0198, Japan*
[3]*Russian Research Centre "Kurchatov Institute," 123182 Moscow, Russia*

(Received 20 October 2010; published 9 August 2011)

The momentum average approximation is used to derive a new kind of nonperturbational analytical expression for the optical conductivity (OC) of a Holstein polaron at zero temperature. This provides insight into the shape of the OC, by linking it to the structure of the polaron's phonon cloud. Our method works in any dimension, properly enforces selection rules, can be systematically improved, and also generalizes to momentum-dependent couplings. Its accuracy is demonstrated by a comparison with the first detailed set of three-dimensional numerical OC results, obtained using the approximation-free diagrammatic Monte Carlo method.

DOI: 10.1103/PhysRevLett.107.076403 PACS numbers: 71.38.−k, 63.20.kd, 72.10.Di

Although the study of polarons is one of the older problems in solid state physics [1], a full understanding of their properties is still missing. This is especially true for the excited states which influence response functions like the optical conductivity (OC). OC measurements have revealed the role of the electron-phonon (e-ph) coupling in many materials, e.g., cuprates [2] and manganites [3]. In particular, the shape of the OC curve is important, as it signifies large versus small polaron behavior [4].

The OC of polarons has been studied numerically using exact diagonalization in 1D [5] and for small clusters in higher dimensions (here, finite size effects can be an issue) [6]. There are also some diagrammatic Monte Carlo (DMC) results for the 3D Fröhlich and 2D Holstein models [7]. DMC gives approximation-free results in the thermodynamic limit, but it requires significant computational effort; this is why there are very few DMC OC sets available in the literature. The conceptual problem associated with all numerical methods, however, is that they do not provide much insight for understanding the shape of the OC and its relation to the properties of the polaron. Analytical expressions are needed for this, but most prior work was limited to perturbational regimes [8]. The one exception is work based on the dynamical mean-field theory (DMFT) [9], which, however, ignores current vertex corrections. The consequences are discussed below; here we state only that a complete understanding of the shape of the OC is still not achieved using it.

It is, then, hard to overemphasize the need for an accurate analytical expression establishing a nonperturbative structure of the OC. In this Letter we obtain such an expression using a generalization of the momentum average (MA) approximation. MA was developed for the single-particle Green's function of the Holstein polaron [10] and then extended to more complex models [11], including disorder [12]. It is nonperturbational since it sums all self-energy diagrams, up to exponentially small terms which are discarded. MA becomes exact in various asymptotic limits, satisfies multiple spectral weight sum rules, is quantitatively accurate in any dimension, at all energies for all parameters except in the extreme adiabatic limit, and can be systematically improved [10].

Here we show how to use MA to calculate two-particle Green's functions, needed in response functions like the OC. Besides efficient yet accurate results at any coupling, this finally provides the explanation for the physical meaning of the shape of the OC. Moreover, this MA-based approach generalizes to OC calculations for models with momentum-dependent e-ph coupling [11].

We use the Holstein model [13] as a specific example since some numerical data are available for comparison:

$$\mathcal{H} = \sum_{\mathbf{k}} (\varepsilon_{\mathbf{k}} c_{\mathbf{k}}^{\dagger} c_{\mathbf{k}} + \Omega b_{\mathbf{k}}^{\dagger} b_{\mathbf{k}}) + \frac{g}{\sqrt{N}} \sum_{\mathbf{k},\mathbf{q}} c_{\mathbf{k}-\mathbf{q}}^{\dagger} c_{\mathbf{k}} (b_{\mathbf{q}}^{\dagger} + b_{-\mathbf{q}}).$$

Here, $c_{\mathbf{k}}^{\dagger}$ and $b_{\mathbf{k}}^{\dagger}$ are electron and boson creation operators for a state of momentum $\mathbf{k}$ (the electron's spin is trivial and we suppress its index). The free-electron dispersion $\varepsilon_{\mathbf{k}} = -2t \sum_{i=1}^{d} \cos(k_i a)$ is for nearest-neighbor hopping on a d-dimensional hypercubic lattice of constant a, and the Einstein optical phonons have energy Ω. The last term describes the local e-ph coupling $g \sum_i c_i^{\dagger} c_i (b_i^{\dagger} + b_i)$, written in $\mathbf{k}$ space. All sums over momenta are over the Brillouin zone and we take the total number N of sites to infinity. We set $\hbar = 1$ and $a = 1$ throughout.

For the case we study here, i.e., a single polaron at $T = 0$, the optical conductivity is given by the Kubo formula [14]:

$$\sigma(\omega) = \frac{1}{\omega V} \int_0^{\infty} dt e^{i\omega t} \langle \psi_0 | [\hat{j}^{\dagger}(t), \hat{j}(0)] | \psi_0 \rangle, \qquad (1)$$

with V the volume, $|\psi_0\rangle$ the polaron ground state (GS), and the charge current operator $\hat{j} = 2et \sum_{\mathbf{q}} \sin q c_{\mathbf{q}}^{\dagger} c_{\mathbf{q}}$ is in the

Heisenberg picture. Here, e is the electron charge and q the component of $\mathbf{q}$ parallel to the electric field.

Our main result is that the optical absorption equals

$$\mathrm{Re}[\sigma_{\mathrm{MA}^{(i)}}(\omega)] = \frac{4\pi e^2 t^2}{\omega} \sum_{n\geq 1} P_n^{(i)} f_n^{(i)}(\omega). \tag{2}$$

Here $i \geq 0$ is the level of $\mathrm{MA}^{(i)}$ approximation, denoting an increasing complexity of the variational description of the eigenstates [10]. However, the physical meaning is the same: $P_n^{(i)}$ is the GS probability to have n phonons at the electron site, while $f_n^{(i)}(\omega)$ are spectral functions describing the electron's optical absorption in this n-phonon environment. Equation (2) shows the direct link between the OC and the structure of the polaron's phonon cloud.

Further discussion is provided below. First, we derive Eq. (2) so that the meaning of various quantities becomes clear. Expanding the commutator and doing the integral in Eq. (1), we find $\sigma(\omega) = \sigma_+(\omega) + (\sigma_+(-\omega))^*$, with

$$\sigma_+(\omega) = \frac{i}{\omega V} \langle \psi_0 | \hat{j}\, \hat{G}(\omega + E_0) \hat{j} | \psi_0 \rangle, \tag{3}$$

where $\hat{G}(\omega) = [\omega + i\eta - \mathcal{H}]^{-1}$ with $\eta \to 0_+$, and E_0 is the polaron GS energy. The usual route is to use a Lehmann representation, leading to the well-known formula

$$\sigma(\omega) = \frac{\pi}{\omega V} \sum_n |\langle \psi_0 | \hat{j} | \psi_n \rangle|^2 \delta(\omega + E_0 - E_n) \tag{4}$$

in terms of excited polaron eigenstates $|\psi_n\rangle$, E_n. Instead, we use twice the resolution of identity to rewrite

$$\sigma_+(\omega) = \frac{i(2et)^2}{\omega V} \sum_{\mathbf{q},\mathbf{Q}} \sin q \sin Q \sum_{\alpha,\beta} \langle \psi_0 | c_{\mathbf{q}}^\dagger | \alpha \rangle \times F_{\alpha\beta}(\mathbf{q}, \mathbf{Q}, \omega + E_0) \langle \beta | c_{\mathbf{Q}} | \psi_0 \rangle, \tag{5}$$

where $F_{\alpha\beta}(\mathbf{q}, \mathbf{Q}, \omega) = \langle \alpha | c_{\mathbf{q}} \hat{G}(\omega) c_{\mathbf{Q}}^\dagger | \beta \rangle$. Since $|\psi_0\rangle$ is the polaron GS, $\{|\alpha\rangle\}$ and $\{|\beta\rangle\}$ are phonon-only states. Moreover, because of invariance to translations, their momentum is $-\mathbf{q}$, respectively $-\mathbf{Q}$. Equation (5) is exact.

Consider now these matrix elements within $\mathrm{MA}^{(0)}$, whose variational meaning is to expand polaron eigenstates in the basis $\{c_i^\dagger (b_j^\dagger)^n |0\rangle\}$, $(\forall) i, j, n$ [10,15]. Then, $|\alpha\rangle \to |-\mathbf{q}, n\rangle = \frac{1}{\sqrt{N}} \sum_i e^{-i\mathbf{q}\cdot\mathbf{R}_i} (b_i^\dagger)^n |0\rangle$, since only such states will have finite overlaps in Eq. (5). The sums over α, β are now sums over phonons numbers $n, m \geq 1$. Note that $n, m = 0$ do not contribute to the regular part of $\sigma(\omega)$ since $|-\mathbf{q}, 0\rangle \sim \delta_{\mathbf{q},0}|0\rangle$, and $\sin q \delta_{\mathbf{q},0} \to 0$. They do contribute to the Drude peak, $\mathcal{D}\delta(\omega)$.

The calculation of the single electron Green's functions $F_{nm}(\mathbf{q}, \mathbf{Q}, \omega) = \langle -\mathbf{q}, n | c_{\mathbf{q}} \hat{G}(\omega) c_{\mathbf{Q}}^\dagger | -\mathbf{Q}, m \rangle$ and of the residues $\langle \psi_0 | c_{\mathbf{q}}^\dagger | -\mathbf{q}, n \rangle$ is now carried out. Details are provided in the Supplemental Material [16]. Here, we note that because of the odd $\sin q$, $\sin Q$ terms, only the part of $F_{nm}(\mathbf{q}, \mathbf{Q}, \omega)$ proportional to $\delta_{\mathbf{q},\mathbf{Q}} \delta_{n,m}$ has nonvanishing contribution to Eq. (5), explaining the single sum over $n \geq 1$ in Eq. (2). Finally, the overlap $|\langle \psi_0 | c_{\mathbf{q}}^\dagger | -\mathbf{q}, n \rangle|^2$ is linked to the probability P_n to have n phonons at the electron site in the polaron GS [17]. The P_n expressions are listed in the Supplemental Material [16]. Altogether, we obtain the result of Eq. (2), where

$$f_n^{(0)}(\omega) = \frac{1}{N} \sum_{\mathbf{q}} \sin^2 q \left| \frac{G_0(\mathbf{q}, E_0 - n\Omega)}{\bar{g}_0(E_0 - n\Omega)} \right|^2 [A_0(\mathbf{q}, \omega + E_0 - n\Omega) - A_0(\mathbf{q}, -\omega + E_0 - n\Omega)], \tag{6}$$

with $A_0(\mathbf{q}, \omega) = -\frac{1}{\pi} \mathrm{Im} G_0(\mathbf{q}, \omega)$ being the free-electron spectral weight, where $G_0(\mathbf{q}, \omega) = (\omega + i\eta - \varepsilon_{\mathbf{q}})^{-1}$. Within the n-phonon sector of $|\psi_0\rangle$, the electron can carry any momentum $\mathbf{q}$ and $f_n^{(0)}(\omega)$ basically describes its optical absorption in the presence of this phonon environment.

At the $\mathrm{MA}^{(1)}$ level, the variational basis is supplemented with the states $\{c_i^\dagger (b_j^\dagger)^n b_l^\dagger |0\rangle\}$, $(\forall) i, j \neq l, n$, which are key to describing the polaron + one-phonon continuum [10]. This enlarges the $\{|\alpha\rangle\}$ and $\{|\beta\rangle\}$ sets with the states $|-\mathbf{q}, n, \delta\rangle = \frac{1}{\sqrt{N}} \sum_i e^{-i\mathbf{q}\cdot\mathbf{R}_i} (b_i^\dagger)^n b_{i+\delta}^\dagger |0\rangle$ for all $\delta \neq 0$. The new matrix elements are found similarly and give much lengthier yet more accurate formulas for $P_n^{(1)}$ and $f_n^{(1)}(\omega)$ [18], but with the same physical meaning.

We now discuss the key features of the 3D OC results. This is because (i) no accurate Holstein OC results were available in 3D, and we provide the first detailed set of DMC data, and (ii) DMFT is a better approximation for higher D. For the OC, the key approximation of DMFT is to ignore current vertex corrections, so we test its validity in 3D where it should be most accurate.

GS phonon probabilities P_n for a 3D Holstein polaron at several effective couplings $\lambda = g^2/(2dt\Omega)$ are shown in Fig. 1. 1D results are quite similar [17]. At weak e-ph couplings, the polaron has few phonons in its cloud so $P_{n\geq 1}$ are small. At the crossover to a small polaron at $\lambda \sim 1$, the distribution changes abruptly and dramatically. As $\lambda \to \infty$, $P_n \to \frac{1}{n!} (\frac{g}{\Omega})^{2n} e^{-g^2/\Omega^2}$, the Lang-Firsov (LF)

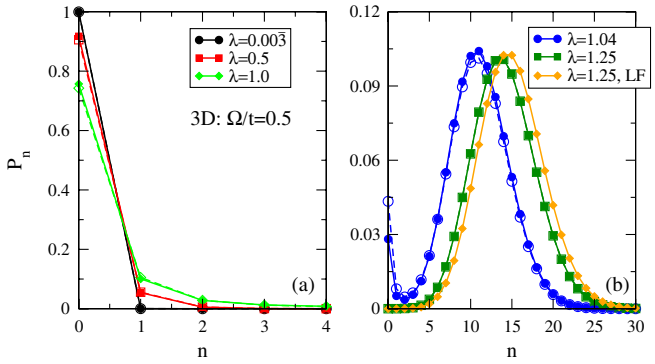

FIG. 1 (color online). Phonon statistics for a 3D Holstein polaron with (a) small to intermediate, and (b) large effective couplings, and $\Omega/t = 0.5$. $\mathrm{MA}^{(0)}$ (dashed lines, open symbols) and $\mathrm{MA}^{(1)}$ (solid lines, solid symbols) results are shown. The Lang-Firsov (LF) asymptotic result is shown for $\lambda = 1.25$.

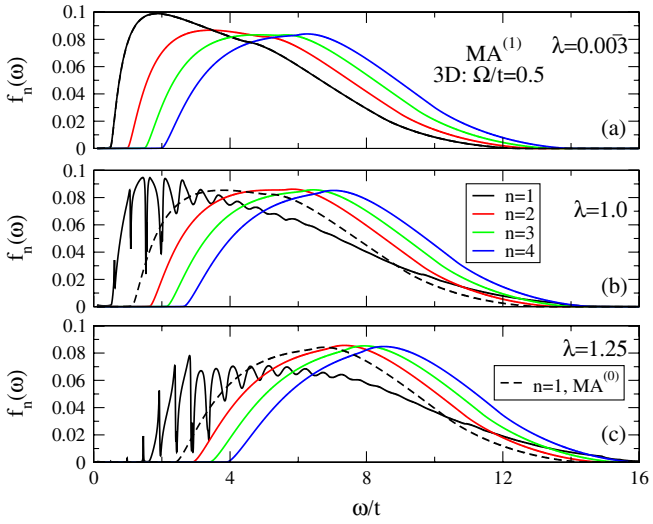

FIG. 2 (color online). $MA^{(1)}$ functions $f_n^{(1)}(\omega)$, for (a) small, (b) medium, and (c) large e-ph coupling, at $\Omega/t = 0.5$, $\eta = 0.005$ in 3D. Also shown is $f_{n=1}^{(0)}(\omega)$ (dashed line).

limit, already quite accurate for $\lambda = 1.25$. The difference between $MA^{(0)}$ and $MA^{(1)}$ is small. This is not surprising, since these probabilities are for the GS, which is already very accurately described by $MA^{(0)}$ [10]. The additional basis states added at the $MA^{(1)}$ level are essential to describe excited states in the polaron + one-phonon continuum, starting at Ω above the GS, and due to a phonon excited far from the polaron cloud [10]. As we show now, they do have a significant effect on the $f_n(\omega)$ functions and therefore on the OC onset.

The ω dependence of the OC is dictated by $f_n(\omega)$. Equation (6) shows that $f_n^{(0)}(\omega)$ becomes finite at $\omega + E_0 - n\Omega \geq -2dt$, because the free-electron spectral weight is finite in $[-2dt, 2dt]$. This implies that the onset of absorption is set by the $n = 1$ curve to be $\omega_{\text{th}} = -2dt - E_0 + \Omega$, and larger n contributions are shifted $(n-1)\Omega$ higher. As λ increases and E_0 falls further below $-2dt$, this suggests that ω_{th} increases monotonically. This is wrong: the OC onset is always expected at $\omega_{\text{th}} = \Omega$ [5,7]. The discrepancy is easy to understand. The onset is due to absorption into the polaron + one-phonon continuum, which is not described by $MA^{(0)}$, only by $MA^{(1)}$ and higher levels [10]. Indeed, as shown in Fig. 2, there is a significant difference between the corresponding $n = 1$ curves, and $f_{n=1}^{(1)}(\omega)$ does have an onset at $\omega_{\text{th}} = \Omega$ even though it becomes hard to see at larger λ. The $n \geq 2$ curves are much less affected, in particular, their onset roughly agrees with that predicted at $MA^{(0)}$ level. Similar behavior is found in 1D, but the peak in each $f_n(\omega)$ moves towards the low-energy threshold [18], as expected since the 1D free-electron density of states is singular at the band edge.

In Fig. 3, we plot a complete set of OC curves for a 3D Holstein polaron, using both MA and DMC methods. On the whole, the agreement is excellent, especially between $MA^{(1)}$ and DMC. We find that $MA^{(1)}$ captures all the qualitative features of the full OC, as well as being able to resolve finer structure near the absorption onset. In particular, the "shoulder" that develops on the low-energy end of the OC spectrum could never be captured with perturbational methods. In the asymptotic $\lambda \to 0, \infty$ limits the curves are nearly indistinguishable, as expected since MA becomes exact in these limits. In the crossover regime $\lambda \sim 1$, the differences between $MA^{(0)}$ and $MA^{(1)}$ are largest, as are those between MA and DMC results. Nevertheless, MA does a good job overall, especially considering that it is an efficient analytical approximation.

The shapes of the OC curves can now be understood using Eq. (2) and the data shown in Figs. 1 and 2. For small λ, $P_{n=1}$ is dominant and the OC is basically proportional to $f_{n=1}(\omega)$. Indeed, its rich structure is clearly visible in the OC, as is its threshold $\omega_{\text{th}} = \Omega$. The $n \geq 2$ terms serve only to alter the high-energy tail. In the small polaron limit, however, $P_{n=1} \to 0$ and the OC is dominated by large n contributions. Since these $f_n(\omega)$ curves have similar shapes and are shifted by Ω with respect to one other, the OC mirrors the LF Poissonian distribution of P_n. The peak location is also in good agreement with $2|E_0| = 12\lambda t$, expected as $\lambda \to \infty$ [8]. This is because

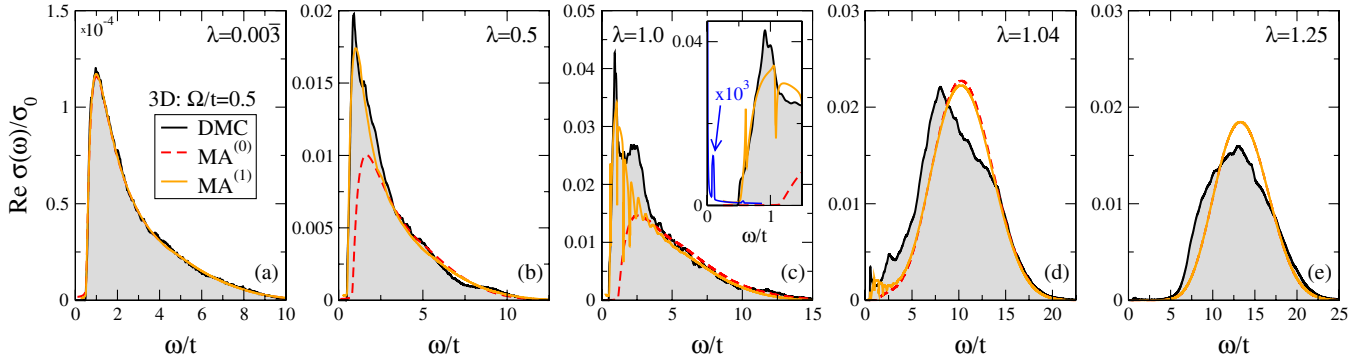

FIG. 3 (color online). OC in units of $\sigma_0 = \pi e^2 t^2$ for a 3D Holstein polaron, calculated using $MA^{(0)}$, $MA^{(1)}$, and DMC. The inset in panel (c) shows the absorption onset, and the no-vertex correction OC at $k_B T = 0.01\Omega$, scaled by 10^3 (thin line marked by arrow).

TABLE I. Total integrated OC $S(\infty)/\sigma_0$ for the parameters used in Fig. 3, for $MA^{(0)}$, $MA^{(1)}$, and DMC.

$\lambda =$	$0.00\bar{3}$	0.5	1.0	1.04	1.25
$MA^{(0)}$	0.0003	0.037	0.084	0.180	0.145
$MA^{(1)}$	0.0003	0.048	0.107	0.180	0.145
DMC	0.0003	0.050	0.125	0.190	0.150

when the electron is moved to a neighboring site by optical absorption, it loses the polaronic binding energy E_0 and it also leaves behind excited phonons with the same energy. The structure of our expression (2) proves that not only the peak energy, but also the very shape of the OC curve is determined by the probabilities $P_n^{(i)}$. In 1D (not shown), the $f_n(\omega)$ functions are more peaked and individual contributions can be seen in the OC, as Ω-spaced kinks. The agreement with available 1D numerical data is of similar a quality with that of Fig. 3 [18].

Consider now the DMFT-like no-vertex correction approximation, in which the two-particle Green's function in Eq. (3) is replaced by a convolution of polaron spectral weights (for details, see [16]). The scaled result for $\lambda = 1$, $k_B T = 0.01\Omega$, is shown in Fig. 3(c). A prominent feature is the peak (marked by an arrow) below ω_{th}, in agreement with low-T data in Ref. [9], where it was identified as an excitation from the GS into the first bound state. Indeed, the peak is at $\sim 0.12t$, their energy difference. The peak likely vanishes at $T = 0$, $\eta = 0$, [16]; however, this shows that a naive consideration of the convolution may lead to a qualitatively wrong idea of the OC structure. DMC and MA results do not show this peak, although the second bound state is visible in their spectral weight [16]. Its absence implies a vanishing matrix element in Eq. (4), likely due to the different symmetry of the polaron wave function in the two states [19]. Clearly, Eq. (2) properly accounts for such selection rules. More analysis is provided in the Supplemental Material [16].

To further prove the accuracy of MA, we compare in Table I the total integrated OC, $S(\infty) = \int_0^\infty d\omega \sigma(\omega)$, for MA and DMC. The agreement is again very good, particularly at small and large λ, where we typically find less than a 5% difference. At intermediate couplings MA accounts for over 85% of the total integrated OC, which is quite remarkable for an analytical approximation.

Knowledge of the total integrated OC can also be used to verify that MA satisfies the f-sum rule, given by [20]:

$$-e^2 a E_{\text{kin}} = \frac{1}{\pi}\mathcal{D} + \frac{2}{\pi}S(\infty), \tag{7}$$

where E_{kin} is the GS polaron kinetic energy and $\mathcal{D} = \pi e^2 a/m^*$ is the Drude weight [21], m^* being the polaron effective mass. Both these quantities can be calculated from the GS properties of the polaron, using known MA methods [10]. In all cases reported here, we have verified that the total integrated OC matches the expected value from the f-sum rule to at least three decimal places.

In conclusion, we have obtained the first accurate analytical nonperturbational expression for the $T = 0$ optical conductivity of a Holstein polaron. It explains the shape of the OC curve by explicitly relating it to the statistics of the polaron cloud. We find no absorption below the threshold at Ω even if a second bound state exists, proving that Eq. (2) accounts for selection rules. Moreover, this work can be generalized for OC studies of polaronic systems with momentum-dependent e-ph coupling, and also disorder, in any dimension.

Work supported by NSERC and CIfAR (G. L. G. and M. B.), and RFBR 10-02-00047a (A. S. M.).

[1] L. D. Landau, Phys. Z. Sowjetunion **3**, 644 (1933).
[2] P. Calvani *et al.*, J. Supercond. **10**, 293 (1997).
[3] O. Gunnarsson and O. Rösch, J. Phys. Condens. Matter **20**, 043201 (2008).
[4] Ch. Hartinger *et al.*, Phys. Rev. B **73**, 024408 (2006).
[5] H. Fehske, J. Loos, and G. Wellein, Phys. Rev. B **61**, 8016 (2000); S. El Shawish *et al.*, Phys. Rev. B **67**, 014301 (2003); J. Loos *et al.*, J. Phys. Condens. Matter **19**, 236233 (2007); A. Alvermann, H. Fehske, and S. A. Trugman, Phys. Rev. B **81**, 165113 (2010); G. De Filippis *et al.*, Phys. Rev. B **72**, 014307 (2005).
[6] H. Fehske *et al.*, Z. Phys. B **104**, 619 (1997).
[7] A. S. Mishchenko *et al.*, Phys. Rev. Lett. **91**, 236401 (2003); G. De Filippis *et al.*, Phys. Rev. Lett. **96**, 136405 (2006); A. S. Mishchenko *et al.*, Phys. Rev. Lett. **100**, 166401 (2008).
[8] For example, see D. Emin, Adv. Phys. **24**, 305 (1975).
[9] S. Fratini, F. de Pasquale, and S. Ciuchi, Phys. Rev. B **63**, 153101 (2001); S. Fratini and S. Ciuchi, Phys. Rev. B **74**, 075101 (2006).
[10] M. Berciu and G. L. Goodvin, Phys. Rev. B **76**, 165109 (2007); M. Berciu, Phys. Rev. Lett. **98**, 209702 (2007).
[11] G. L. Goodvin and M. Berciu, Phys. Rev. B **78**, 235120 (2008); M. Berciu and H. Fehske, Phys. Rev. B **82**, 085116 (2010); D. Marchand *et al.*, Phys. Rev. Lett. **105**, 266605 (2010).
[12] M. Berciu, A. S. Mishchenko, and N. Nagaosa, Europhys. Lett. **89**, 37007 (2010); G. L. Goodvin, L. Covaci, and M. Berciu, Phys. Rev. Lett. **103**, 176402 (2009).
[13] T. Holstein, Ann. Phys. (N.Y.) **8**, 325 (1959).
[14] G. D. Mahan, *Many Particle Physics* (Plenum, NY, 1981).
[15] O. S. Barisic, Phys. Rev. Lett. **98**, 209701 (2007).
[16] See Supplemental Material at http://link.aps.org/supplemental/10.1103/PhysRevLett.107.076403 for more details on the calculations and DMFT comparison.
[17] M. Berciu, Can. J. Phys. **86**, 523 (2008).
[18] G. L. Goodvin and M. Berciu (unpublished).
[19] O. S. Barisic, Phys. Rev. B **69**, 064302 (2004); B. Lau, M. Berciu, and G. A. Sawatzky, Phys. Rev. B **76**, 174305 (2007).
[20] P. F. Maldague, Phys. Rev. B **16**, 2437 (1977).
[21] W. Kohn, Phys. Rev. **133**, A171 (1964).